IEEE Access
Multidisciplinary | Rapid Review | Open Access Journal

Received 23 September 2022, accepted 10 October 2022, date of publication 20 October 2022, date of current version 8 November 2022.

Digital Object Identifier 10.1109/ACCESS.2022.3215492

RESEARCH ARTICLE

Robust 2-D DOA Estimation in a Polarization Sensitive Single User Environment

MD IMRUL HASAN, (Student Member, IEEE), AND MOHAMMAD SAQUIB, (Senior Member, IEEE)
Department of Electrical Engineering, The University of Texas at Dallas, Richardson, TX 75080, USA
Corresponding authors: Md Imrul Hasan (mdimrul.hasan@utdallas.edu) and Mohammad Saquib (saquib@utdallas.edu)

ABSTRACT Apart from the conventional parameters (such as signal-to-noise ratio (SNR), array geometry and size, and the number of samples), several other factors (e.g., alignment of the antenna elements, polarization parameters) influence the performance of direction of arrival (DOA) estimation algorithms. When all the antenna elements are aligned in the same direction, the polarization parameters uniformly affect the steering vectors, which is the underlying assumption of almost all conventional DOA algorithms. Unfortunately, in this case, for a given set of DOA angles, there exists a range of polarization parameters resulting in a very low SNR across all the antenna elements in the array and vice versa. To avoid this type of unwanted event, different antenna elements must be aligned differently. However, this fact will make almost all commonly used DOA estimation algorithms inoperable since the steering vectors are contaminated unevenly by the polarization parameters. To the best of our knowledge, no work in the literature handles this issue using simple hardware and signal processing techniques even for a single user environment. In this paper, that line of inquiry is pursued. We consider a circular array with the minimum number (i.e., 4) of short dipole antenna elements and propose an antenna alignment scheme. This ensures that at any given point no more than one element will suffer significantly from low SNR due to the contribution of polarization. A thresholding technique to isolate the antenna element after being seriously contaminated by the polarization parameters is developed and analyzed. Two algorithms that are suited for operating reliably in all possible DOA and polarization environments are addressed. The first algorithm follows the working principle of the popular MUSIC algorithm after cleaning the polarization contributions from the non-signal subspace. The other one, which is found as a byproduct of the process of cleaning the non-signal subspace, can estimate the DOA angles in a closed form manner. The implementations of the above algorithms for an arbitrary number of antenna elements greater than or equal to 4 are also presented. Finally, a thorough performance and complexity analysis are illustrated for those two algorithms considering various polarization and DOA scenarios.

INDEX TERMS DOA estimation, polarization, closed-form estimation, MUSIC, antenna alignment, antenna mapping.

I. INTRODUCTION

Direction of arrival (DOA) is a key issue in various important applications, such as sonar, radar, medical sector, astronomy, defense operations, navigation, geophysics, acoustic tracking, and so on [1], [2], [3], [4], [5]. Nowadays, owing to the exceptional development of modern technology and smart devices, DOA estimation techniques have been widely used in wireless communication and the internet of things (IoT) [6], [7], [8], [9], [10]. The localization of a single narrow-band source by a passive sensor array has also attracted tremendous interest in the literature due to its numerous applications [11], [12], [13], [14], [15], [16], [17], [18]. Over several decades, extensive studies have been

The associate editor coordinating the review of this manuscript and approving it for publication was Fabrizio Santi.

This work is licensed under a Creative Commons Attribution 4.0 License. For more information, see https://creativecommons.org/licenses/by/4.0/

performed, and numerous algorithms have been developed to estimate the DOAs, i.e., multiple signal classification (MUSIC) [19], maximum-likelihood (ML) [20], Capon [21], estimation of signal parameters via rotational invariance techniques (ESPRIT) [22], Min-Norm [23], etc. Among all these methods, the MUSIC algorithm is especially noteworthy due to its easy implementation with different array structures. Antenna array geometry also plays an important role while implementing the DOA estimation algorithms. To estimate the DOAs, linear array geometry is extensively studied in the literature [24], [25], [26]. However, the important drawback of a linear antenna array is the 1-D angle scanning. The circular antenna array (UCA) is offered to overcome the problem owing to its advantage of providing 360-degree azimuthal coverage as well as the elevation information of the DOAs [27], [28], [29], [30], [31].

The performance of the existing DOA estimation algorithms is mostly demonstrated by assuming mismatch-free steering elements. However, those suffer greatly when the steering elements are corrupted. Significant efforts [32], [33], [34], [35], [36], [37], [38], [39], [40] have been made to handle this issue and perform robust beamforming. There are various reasons for steering element mismatch, such as look direction and signal pointing errors [32], [33], imperfect array calibration, distortion of antenna shape [34], source wavefront distortions resulting from environmental inhomogeneities [35], [36], the near-far problem [37], source spreading, and local scattering [38]. In [39] and [40], the uncertainties in a steering vector are tackled by modeling them as a Gaussian random vector. The steering elements can also be corrupted by the polarization parameters. These cause a twofold effect by contaminating the phase of each steering term as well as affecting the received power of the corresponding antenna element. Unlike the other imperfections associated with steering elements, the polarization effects depend on the polarization parameters, the alignments of the antenna elements, and DOA angles. This fact calls for the joint design of an antenna alignment scheme and robust 2-D DOA estimation algorithms in an arbitrary polarization environment.

The polarization sensitivity of the array to incident signals must be considered in the DOA estimation. The received signal power is greatly affected by polarization while forming a transmitter-receiver pair. When the polarization of the receiver antenna matches the transmitter antenna's polarization, the receiver collects the signal with the maximum possible power. On the other hand, a polarization mismatch between the transmitter-receiver pair can result in severe degradation of the received signal power. The polarization of the transmitter can be previously known; however, the polarization state of the transmitted signal can change when the electromagnetic wave scatters from a target [41], [42]. Under the Born approximation, different polarizations of the electromagnetic waves are affected differently depending on the geometrical and dielectric properties of the target, which are usually unknown in a practical environment [43]. Due to the unpredictability of the received signal's polarization state, keeping all the antenna elements in the same direction to match the polarization of the transmitter can often cause to receive the signal with a very low signal-to-noise ratio (SNR). Contrarily, using different directions for different antennas will affect the elements of the steering vector differently. This could lead the regular DOA estimation algorithms to exhibit unreliable performance.

In the existing literature, no work directly addresses the polarization contamination considering all possible polarization scenarios which is the main motivation of this paper. Nevertheless, two kinds of strategies can be employed in the developed works to bypass the effects of polarization to estimate the DOAs. The works in [44], [45], [46], [47], and [48] use complex hardware which can be utilized to handle this issue by choosing the same aligned set of antenna elements with the highest received signal power. In [44], a uniform linear array with crossed dipoles is used to jointly estimate the DOAs and the polarization parameters implementing the ESPRIT algorithm. The MUSIC algorithm of joint polarization-DOA estimation based on the polarization-sensitive circular array with a crossed dipole is discussed in [45]. A uniform linear crossed tripole array is introduced for a dimension-reduction-based MUSIC algorithm in [46]. [47] and [48] perform the estimation using a circular vector sensor array comprising of co-centered orthogonal loop and dipole (COLD). However, they require the same phase center for the corresponding cross dipole/tripole/COLD antennas which remains a challenge. In this case, those elements are also greatly affected by mutual coupling. The second strategy can be to face all the antenna elements in the same direction [49] which may cause them to suffer from low SNR due to the contribution of the polarization.

In this paper, we present how to localize a single narrowband source using a UCA of simple short dipole antenna elements just employing signal processing techniques. Here, we want to utilize the minimum number of antenna elements, and at the same time, ensure that no more than one antenna element suffers significantly from low received power or SNR owing to the contribution of polarization. This fact leads us to mathematically develop an antenna alignment scheme, which also helps us to easily cancel the effects of polarization from the non-signal subspace while implementing the popular MUSIC algorithm. The entire algorithm is referred to as C-MUSIC. While cleansing the non-signal subspace for MUSIC, we develop a reduced complexity algorithm, namely CF that estimates the DOA angles in a closed-form manner. The other major contributions of this paper can be outlined as follows:

1) As claimed, under the proposed antenna element alignment scheme, no more than one element will suffer from very low received power due to the polarization contribution. A decision threshold K is introduced to decide whether the antenna element with the smallest

received power should be considered in the process of DOA estimation or not.

a) Two methods are developed to design the threshold K. The 1st method is based on the well-known Neyman-Pearson lemma and the 2nd one is based on the central limit theorem (CLT).
b) An extensive probabilistic analysis of K is performed in order to provide significant insights into the impact of K on the system performance.

2) Two non-signal subspace cleansing methods are demonstrated for C-MUSIC.
   a) One of the methods can be employed only when the smallest received power among all the antenna elements is below the threshold K. The other one applies to all possible received power scenarios.
3) A through performance and complexity study is performed between C-MUSIC and CF algorithms.

The rest of the paper is organized as follows: Section II presents the system model. In Section III, the problem statement is formulated and the DOA estimation algorithms (C-MUSIC and CF) are developed in Section IV assuming no background noise. Implementations of those algorithms in a noisy arbitrarily polarized environment are discussed in Section V with analysis. In Section VI, the numerical results are presented. Section VII discusses the applications and future works, and finally, the concluding remarks of this paper are given in Section VIII.

Notations: We use lowercase and uppercase bold letters to denote vectors and matrices, respectively. Lowercase letters in italics are used to represent scalars. The notation * refers to the complex conjugate of a scalar, $[\cdot]^T$ refers to transpose, and $[\cdot]^\dagger$ denotes the Hermitian of a matrix.

II. SYSTEM MODEL

Let us consider a UCA of radius r composed of arbitrarily aligned N identical short dipole antennas. The elements are positioned on the circumference of the circle on the $xy-$plane where the first element is located on the $x-$axis; see Figure 1. These surface antenna elements are low profile, easily mountable, and very robust on a rigid surface [50], [51]. The incident signal at the array is a complex unknown narrow-band signal $s(m)$ coming from a far field source. The azimuthal angle ϕ of this signal is measured counterclockwise from the $x-$axis, and the elevation angle θ is measured downward from the $z-$axis; where $0^\circ \leq \phi < 360^\circ$ and $0^\circ \leq \theta \leq 90^\circ$. The signal is arbitrarily polarized, where $0^\circ \leq \eta < 360^\circ$, and $0^\circ \leq \gamma \leq 90^\circ$ represent the polarization phase difference, and the auxiliary polarization angle, respectively. These terms satisfy $\tan\gamma = A_y/A_x$, and $\eta = \phi_y - \phi_x$, where, A_y and ϕ_y are the electric field amplitude and the electric field phase along the $y-$axis, respectively, and A_x, and ϕ_x are defined accordingly for $x-$axis [52].

The output voltage from each short dipole is proportional to the electric field component along the dipole axis and the length of the dipole [53]. Hence, the outputs of these identical

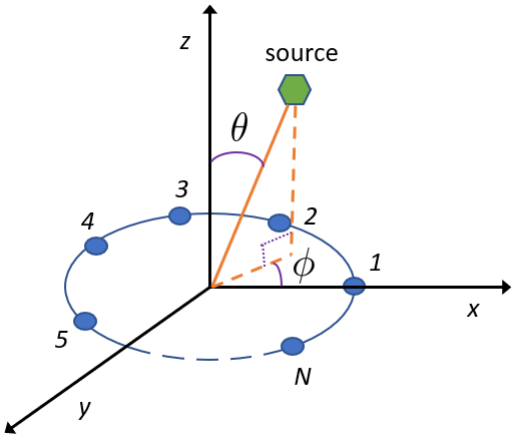

FIGURE 1. Uniform circular array geometry.

elements parallel to the x, and y axes will be proportional to the x, and y components of the electric field, respectively. According to [48] and [53], the electric fields along x, and y axes are given by

$$\begin{bmatrix} e_x \\ e_y \end{bmatrix} = \begin{bmatrix} e^{j\eta}\sin\gamma\cos\theta\cos\phi - \sin\phi\cos\gamma \\ e^{j\eta}\sin\gamma\cos\theta\sin\phi + \cos\phi\cos\gamma \end{bmatrix}. \tag{1}$$

At the n^{th} dipole antenna element, the output voltage is proportional to the electric field

$$\begin{aligned} e_n &= e^{j\eta}\sin\gamma\cos\theta\cos(\phi-\zeta_n) - \sin(\phi-\zeta_n)\cos\gamma \\ &= e_x\cos\zeta_n + e_y\sin\zeta_n, \end{aligned} \tag{2}$$

where ζ_n is the alignment angle of that element w.r.t. the $x-$axis; see Figure 2. Notice in (2) that the electric field components e_x, and e_y of (1) are special cases of e_n for $\zeta_n = 0^\circ$, and $\zeta_n = 90^\circ$, respectively. Equation (2) also implies that for $\theta = 90^\circ$, and $\gamma = 90^\circ$, irrespective of any antenna alignment angle ζ_n, the received signal power (RSP) $= 0$ at all the antenna elements due to the electric field $e_n = 0$. If that is the case, we decide the source is along the $xy-$plane, since $\theta = 90^\circ$, and the value of ϕ can not be determined. This situation can be overcome by having one or more short dipole antenna elements along the $z-$axis at the cost of losing the low profile and very robust properties of the surface antenna elements, which is beyond the scope of this paper. Throughout the rest of this paper, we consider $\theta \neq 90^\circ$ or $\gamma \neq 90^\circ$ which is equivalent to $e_x \neq 0$ or $e_y \neq 0$.

The steering term for the n^{th} element shown in Figure 1 relates to the source's DOA angles (θ, ϕ) as

$$a_{s_n} = e^{j\frac{2\pi}{\lambda}r\sin\theta\cos(\phi-\beta_n)}, \tag{3}$$

where $\beta_n = 2\pi(n-1)/N$; $n = 1, 2, 3, \ldots, N$, and λ denotes the wavelength of the target signal. The array manifold term for the n^{th} antenna element can be written as the product of the associated electric field response and the steering terms [47], [48], [52] as

$$a_n = e_n a_{s_n}. \tag{4}$$

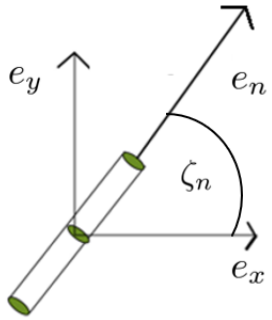

FIGURE 2. Electric field in a short dipole antenna.

At the m^{th} snapshot, the output of element n is

$$x_n(m) = a_n s(m) + w_n(m), \tag{5}$$

where $w_n(m)$ is zero-mean white complex Gaussian noise with average power σ^2, and spatially and temporally independent of $s(m)$.

Now collecting outputs from all N antenna elements, we form:

$$\mathbf{x}(m) = \mathbf{a}s(m) + \mathbf{w}(m), \tag{6}$$

where

$$\mathbf{a} = \begin{bmatrix} a_1 \\ a_2 \\ \vdots \\ a_N \end{bmatrix}; \quad \mathbf{x}(m) = \begin{bmatrix} x_1(m) \\ x_2(m) \\ \vdots \\ x_N(m) \end{bmatrix}; \quad \mathbf{w}(m) = \begin{bmatrix} w_1(m) \\ w_2(m) \\ \vdots \\ w_N(m) \end{bmatrix}. \tag{7}$$

Equation (6) will be processed to extract the desired DOA information using C-MUSIC and CF algorithms.

III. PROBLEM FORMULATION: LIMITATIONS OF MUSIC

Let us begin with a short description of the subspace-based 2-D MUSIC algorithm. It exploits the eigenstructure of the auto-correlation matrix of the received signal (6), which is

$$\begin{aligned} \mathbf{R} &= \mathbb{E}\{\mathbf{x}(m)\mathbf{x}(m)^\dagger\} \\ &= \mathbf{a}s(m)s(m)^\dagger\mathbf{a}^\dagger + \mathbb{E}\{\mathbf{w}(m)\mathbf{w}(m)^\dagger\} \\ &= \sigma_{s,m}^2\mathbf{a}\mathbf{a}^\dagger + \sigma^2\mathbf{I}, \end{aligned} \tag{8}$$

where $\sigma_{s,m}^2 = |s(m)|^2$, $\mathbb{E}\{\mathbf{w}(m)\mathbf{w}(m)^\dagger\} = \sigma^2\mathbf{I}$, and $\mathbf{I}$ is an $N \times N$ identity matrix. Note that in (8), the expectation is the conditional expectation over the noise sequence, and as a result, the signal power depends on time index m. In practice, the above auto-correlation matrix will be replaced by the sample auto-correlation matrix averaged over M time samples (or snapshots). Since a single source is considered, the largest eigenvalue of this auto-correlation matrix is corresponding to the signal subspace. The others are corresponding to the non-signal (or noise) subspace which is defined as

$$\mathbf{E} = [\mathbf{v}_2, \mathbf{v}_3, \cdots, \mathbf{v}_N], \tag{9}$$

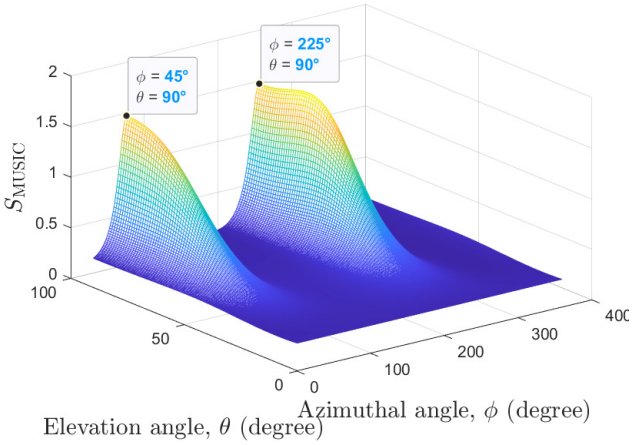

FIGURE 3. MUSIC spectrum in a polarization-sensitive environment.

where $\{\mathbf{v}_l\}_{l=1}^N$ denotes the eigenvector corresponding to the real eigenvalue $\{\lambda_l\}_{l=1}^N$ of $\mathbf{R}$. These eigenvalues are sorted in descending order. Using the noise subspace $\mathbf{E}$ (9), the MUSIC spectrum is defined as [54]

$$S_{\text{MUSIC}} = \frac{1}{\mathbf{a}^\dagger\mathbf{E}\mathbf{E}^\dagger\mathbf{a}}. \tag{10}$$

Next, we discuss the implementation requirement of the MUSIC algorithm in an arbitrarily polarized environment. MUSIC needs at least two eigenvectors in the noise subspace in order to estimate two DOA angles (azimuthal and elevation) unambiguously. Therefore, the minimum required number of antenna elements is three. Due to the polarization and DOA angles, the compound steering element a_n may be (close to) 0 in (4) at one (or more) antenna elements depending on the alignment. This would result in very low signal power. The example below describes such an unwanted situation.

Let us assume a three element UCA where all the elements are aligned along the $x-$ axis, and the incoming wave arrives with the azimuthal angle $\phi = 90°$, and the auxiliary polarization angle $\gamma = 90°$. This set of parameters yields received electric field response $e_n = e_x = 0$, hence $a_n = 0$, for all n which leads the received signal in (6) to be zero in the noiseless scenario. In this situation, no regular DOA estimating algorithm will be able to operate.

To resolve this issue, one must use at least four element UCA with different alignments for different elements such that the above harmful event (i.e., $a_n = 0$) can't affect more than one antenna element.

Unfortunately, a four-element UCA with different alignments is not even enough for the conventional MUSIC to operate. It is due to the fact that the conventional MUSIC assumes $e_n = e_{n'}$ for $n \neq n'$ in (2), that results the non-signal subspace free from the contribution of the polarization parameters. It is not true when the antenna elements are aligned differently. At the n^{th} element, the compound term in (4) can be written as

$$a_n = e_n a_{s_n} = |e_n|e^{j\delta_n}|a_{s_n}|e^{j\psi_n}, \tag{11}$$

where $|a_{s_n}| = 1$. Terms δ_n and ψ_n are the phases of electric field response e_n, and steering element a_{s_n}, respectively. The element (p, q) of the auto-correlation matrix $\mathbf{R}$ is $\sigma^2_{s,m}|e_p||e_q|e^{j(\delta_{p,q}+\psi_{p,q})}$, where $\delta_{p,q} = \delta_p - \delta_q$, and $\psi_{p,q} = \psi_p - \psi_q$. Since all the antenna elements have different alignments, $e_p \neq e_q$ for $p \neq q$ and therefore, different elements of the auto-correlation matrix $\mathbf{R}$ are affected by the polarization parameters differently. This forces the associated non-signal subspace to deviate from the desired one, which is free from the polarization parameters. This will cause failure of the MUSIC algorithm; see Figure 3, where MUSIC spectrum is plotted using the DOA angle pair, $\theta = 30°$, $\phi = 60°$, and the polarization parameter pair, $\gamma = 45°$, $\eta = 45°$, and alignment angle of antenna element n, $\zeta_n = (n-1) \times 30°$, where $n = 1, 2, 3, 4$. More discussion and analysis on this issue will be found in the following section. Note that MUSIC performs perfectly fine for the above set of DOA and polarization angles if all the antenna elements are aligned in the same direction (i.e., $\zeta_n = \zeta_{n'}$ for $n \neq n'$). However, this same alignment could result in an unwanted incident for a different set of DOA and polarization angles as demonstrated in the earlier example.

The above two examples jointly suggest that in a single user arbitrarily polarized environment to find the DOA angles, different alignments must be used for different antenna elements, and the implementation of MUSIC requires cleansing of the polarization parameters from the non-signal subspace. Thus, in this work MUSIC is referred to as C-MUSIC, where the alphabet 'C' stands for the additional signal processing task (i.e., cleansing operation of the polarization contribution) performed prior to implementing the conventional MUSIC algorithm. In the following section, we will also demonstrate that after cleansing, how one can estimate the DOA angles in a closed-form manner using the CF algorithm.

IV. ESTIMATION OF THE DOA ANGLES: C-MUSIC AND CF

Before starting elaborating upon the C-MUSIC and CF algorithms, let us derive the antenna alignment guideline to ensure that the effects of the polarization should not be able to hurt more than one antenna element in terms of RSP as long as $e_x \neq 0$ or $e_y \neq 0$. In that regard, the following theorem would be useful.

Theorem 1: If antenna elements n and $n' \neq n$ are aligned such that $\zeta_{n'} \neq \zeta_n$ or $\zeta_{n'} \neq \zeta_n \pm 180°$, the RSP can't be simultaneously zero at antenna n and n' when $e_x \neq 0$ or $e_y \neq 0$.

Proof: Let us assume RSP $= 0$ at antenna element n and equivalently from (2), we get the received electric field response at antenna n

$$e_n = e_x \cos\zeta_n + e_y \sin\zeta_n = 0. \tag{12}$$

Without loss of generality, we can write the alignment angle of antenna $n' \neq n$ as

$$\zeta_{n'} = \zeta_n + \zeta, \tag{13}$$

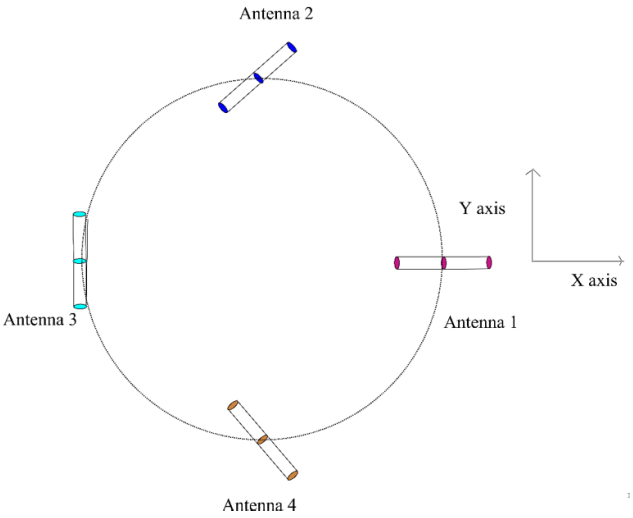

FIGURE 4. Proposed antenna alignment scheme for a UCA with $N = 4$.

where $0 \leq \zeta < 360°$. Applying the above equation and (12), to (2), and after simplification, the received electric field response at antenna n' becomes

$$e_{n'} = \sin\zeta \left(e_x \sin\zeta_n - e_y \cos\zeta_n\right). \tag{14}$$

If $e_x \neq 0$ or $e_y \neq 0$, (12) implies

$$e_x \sin\zeta_n - e_y \cos\zeta_n \neq 0,$$

equivalently

$$e_{n'} \neq 0,$$

unless $\zeta = 0$ (i.e., $\zeta_{n'} = \zeta_n$) or $\pm 180°$ (i.e., $\zeta_{n'} = \zeta_n \pm 180°$) in (13). This proves the theorem. ■

Condition $\zeta_{n'} \neq \zeta_n$ for $n' \neq n$ in Theorem 1 implies that all 4 antenna elements must be aligned differently. In addition, if we choose the antenna element alignment such that $0° \leq \zeta_n < 180°$ for all n, the other requirement $\zeta_{n'} \neq \zeta_n \pm 180°$ for $n' \neq n$ in Theorem 1 will be met. One such array that meets both criteria of Theorem 1 is depicted in Figure 4. Here, it can be seen that antennas 1 and 3 are aligned along the x and y axes, respectively, and antennas 2 and 4 are aligned by 45°, and 135°, respectively, with respect to the $x-$axis. C-MUSIC and CF algorithms now will be developed using the above antenna element alignment scheme.

A. C-MUSIC

Theorem 1 and the antenna alignment scheme given in Figure 4 jointly result in five different RSP scenarios in the presence of a target. We categorize those scenarios into two primary cases. In Case 1, $a_n = 0$ only at antenna element n; since $n = 1, 2, 3, 4$, there are four sub-cases. Term $\Omega_{1,n}$ represents the $n^{\underline{\text{th}}}$ sub-case of Case 1. In Case 2 (denoted by Ω_2), $a_n \neq 0$ at all the antenna elements. In practice, Case 2 occurs much more frequently than Case 1, since the former to happen requires a special combination of DOA angles (ϕ and θ) for a given pair of polarization parameters (η and γ). For example, let us assume the incoming signal

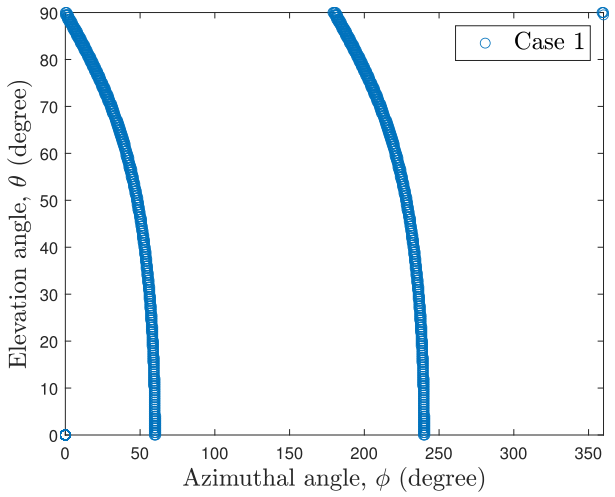

FIGURE 5. DOAs causing Case 1 ($a_1 = 0$) for $\eta = 0°$, and $\gamma = 60°$.

of polarization parameters $\eta = 0°$, and $\gamma = 60°$ excites the UCA array. Figure 5 depicts the values of the elevation angle θ, and the azimuthal angle ϕ that cause $a_1 = 0$ (Case 1, $\Omega_{1,1}$) where the classical array signal processing algorithms yield unreliable estimates of the DOAs.

Nevertheless, the DOA estimation algorithms must operate efficiently in each of the above possible cases. Structures of the signal and non-signal subspace will vary from one case to another. This fact requires a dedicated polarization suppression method for each of the five effective cases. As a result, to apply the right method, the case that has occurred must be correctly identified. For the purpose of demonstration, we assume the perfect detection of the cases given the RSP scenarios at all the antennas. Later, we will present two threshold-based techniques to operate the algorithm in a real-life scenario. Let us begin with Case 1 and demonstrate how to implement C-MUSIC.

1) CASE 1

Firstly, we consider the first sub-case of Case 1, i.e., $\Omega_{1,1}$. At the m^{th} sample, for $\beta_n = 2\pi(n-1)/N$ and $\zeta_n = (n-1) \times 45°$, the received signal in (6) is

$$\mathbf{x}(m) = \mathbf{s}_{\text{t}} s(m) = \begin{bmatrix} 0 \\ \frac{1}{\sqrt{2}} e_y e^{j\kappa_2} \\ e_y e^{-j\kappa_1} \\ \frac{1}{\sqrt{2}} e_y e^{-j\kappa_2} \end{bmatrix} s(m), \tag{15}$$

where $\kappa_1 = \kappa \cos\phi$, $\kappa_2 = \kappa \sin\phi$ and $\kappa = 2\pi r \sin\theta/\lambda$. Removing the first element (i.e., 0) from the original received signal vector, we form a new received signal vector as

$$\tilde{\mathbf{x}}(m) = e_y \tilde{\mathbf{s}}_{\text{t}} s(m), \tag{16}$$

where $\tilde{\mathbf{s}}_{\text{t}} = \begin{bmatrix} \frac{1}{\sqrt{2}} e^{j\kappa_2} & e^{-j\kappa_1} & \frac{1}{\sqrt{2}} e^{-j\kappa_2} \end{bmatrix}^\top$. Note that in the newly formed received signal vector (16), the polarization contributes two multiplicative terms, one is e_y, and the other one is $1/\sqrt{2}$ (in the 1st and 3rd elements of vector $\tilde{\mathbf{s}}_{\text{t}}$). Vector $\tilde{\mathbf{s}}_{\text{t}}$ carries useful information pertaining to the DOAs. For Case 1, C-MUSIC can be implemented in two ways, the first method, namely Method 1, executes by cleaning the non-signal subspace of the auto-correlation matrix of the received signal (16) and, the second method, namely Method 2, operates estimating κ_1 and κ_1. Next, we describe Method 1.

a: METHOD 1

We can write the auto-correlation matrix of the received signal as

$$\tilde{\mathbf{R}} = |e_y|^2 \sigma_{\text{s},m}^2 \tilde{\mathbf{s}}_{\text{t}} \tilde{\mathbf{s}}_{\text{t}}^\dagger = |e_y|^2 \sigma_{\text{s},m}^2 \tilde{\mathbf{R}}_{\text{s}}, \tag{17}$$

where

$$\tilde{\mathbf{R}}_{\text{s}} = \begin{bmatrix} \frac{1}{2} & \frac{1}{\sqrt{2}} e^{j(\kappa_1+\kappa_2)} & \frac{1}{2} e^{2j\kappa_2} \\ \frac{1}{\sqrt{2}} e^{-j(\kappa_1+\kappa_2)} & 1 & \frac{1}{\sqrt{2}} e^{-j(\kappa_1-\kappa_2)} \\ \frac{1}{2} e^{-2j\kappa_2} & \frac{1}{\sqrt{2}} e^{j(\kappa_1-\kappa_2)} & \frac{1}{2} \end{bmatrix}.$$

To develop C-MUSIC, we derive a subspace from $\tilde{\mathbf{R}}$ identical to the non-signal subspace of

$$\tilde{\mathbf{R}}_{\text{s,c}} = \tilde{\mathbf{s}}_{\text{t,c}} \tilde{\mathbf{s}}_{\text{t,c}}^\dagger,$$

where $\tilde{\mathbf{s}}_{\text{t,c}} = \begin{bmatrix} e^{j\kappa_2} & e^{-j\kappa_1} & e^{-j\kappa_2} \end{bmatrix}^\top$ is the clean version of the compounded steering vector $\tilde{\mathbf{s}}_{\text{t}}$ in (16). The above auto-correlation matrix $\tilde{\mathbf{R}}_{\text{s,c}}$ can be shown as

$$\tilde{\mathbf{R}}_{\text{s,c}} = \begin{bmatrix} 1 & e^{j(\kappa_1+\kappa_2)} & e^{2j\kappa_2} \\ e^{-j(\kappa_1+\kappa_2)} & 1 & e^{-j(\kappa_1-\kappa_2)} \\ e^{-2j\kappa_2} & e^{j(\kappa_1-\kappa_2)} & 1 \end{bmatrix}. \tag{18}$$

We now prove the following theorem to derive the non-signal subspace of $\tilde{\mathbf{R}}_{\text{s,c}}$ from $\tilde{\mathbf{R}}$ of (17).

Theorem 2: The non-signal subspace of $\tilde{\mathbf{R}}_{\text{s,c}}$ in (18) is the null space of $\tilde{\mathbf{R}}\mathbf{F}_1$, where $\mathbf{F}_1 = \text{diag}\begin{bmatrix} 1 & \frac{1}{\sqrt{2}} & 1 \end{bmatrix}$.

Proof: Let $\mathbf{v} = \begin{bmatrix} v_1 & v_2 & v_3 \end{bmatrix}^\top$ be a vector belonging to the non-signal subspace of $\tilde{\mathbf{R}}_{s,c}$, then

$$\begin{bmatrix} 1 & e^{j(\kappa_1+\kappa_2)} & e^{2j\kappa_2} \\ e^{j(\kappa_1+\kappa_2)} & 1 & e^{-j(\kappa_1-\kappa_2)} \\ e^{-2j\kappa_2} & e^{j(\kappa_1-\kappa_2)} & 1 \end{bmatrix} \begin{bmatrix} v_1 \\ v_2 \\ v_3 \end{bmatrix} = \begin{bmatrix} 0 \\ 0 \\ 0 \end{bmatrix}. \tag{19}$$

Since $\tilde{\mathbf{R}}\mathbf{F}_1\mathbf{v}$ equals to

$$|e_y|^2 \sigma_{\text{s},m}^2 \begin{bmatrix} \frac{1}{2} & \frac{1}{2} e^{j(\kappa_1+\kappa_2)} & \frac{1}{2} e^{2j\kappa_2} \\ \frac{1}{\sqrt{2}} e^{-j(\kappa_1+\kappa_2)} & \frac{1}{\sqrt{2}} & \frac{1}{\sqrt{2}} e^{-j(\kappa_1-\kappa_2)} \\ \frac{1}{2} e^{-2j\kappa_2} & \frac{1}{2} e^{j(\kappa_1-\kappa_2)} & \frac{1}{2} \end{bmatrix} \times \begin{bmatrix} v_1 \\ v_2 \\ v_3 \end{bmatrix},$$

applying (19) to the above expression, we get

$$\tilde{\mathbf{R}}\mathbf{F}_1\mathbf{v} = \begin{bmatrix}0 & 0 & 0\end{bmatrix}^\top,$$

and we prove the theorem. ■

Next, we find the angles corresponding to the maximum spectrum value in (10) utilizing the null space of $\tilde{\mathbf{R}}\mathbf{F}_1$ and use those as the DOA estimates. Theorem 2 guides us how to obtain the non-signal subspace for implementing C-MUSIC when $a_n = 0$ for $n = 1$. Similarly, when $a_n = 0$ for $n \neq 1$, the auto-correlation matrix $\tilde{\mathbf{R}}$ will be formed discarding the received signal samples from that antenna element. As a result, the structure of $\tilde{\mathbf{R}}$ changes with n that changes the structure of $\mathbf{F}_n$ as follows:

$$\mathbf{F}_2 = \text{diag}\left[1 \quad -1 \quad -\frac{1}{\sqrt{2}}\right]; \quad \mathbf{F}_3 = \text{diag}\left[1 \quad \sqrt{2} \quad -\sqrt{2}\right];$$

and

$$\mathbf{F}_4 = \mathbf{F}_1.$$

The derivations of $\{\mathbf{F}_n\}_{n=2}^4$ are similar to $\mathbf{F}_1$ and omitted for conciseness. Let us focus again on Case 1 due to $a_n = 0$, and elaborate upon Method 2.

b: METHOD 2

The following lemma, which can be straightforwardly obtained from (15), forms the basis for this method.

Lemma 1: The phase parameters $\{\kappa_i\}_{i=1}^2$ of the steering elements can be derived from each sample of the received signal vector $\tilde{\mathbf{x}}(m)$ in (15) as

$$\kappa_2 = \frac{1}{2}\angle\{x_2(m)x_4^*(m)\},$$

and

$$\kappa_1 = \angle\{x_2(m)x_3^*(m)\} - \kappa_2.$$

In a noisy environment, applying Lemma 1 to each sampled received signal, and then averaging those over M samples, we get the estimates of κ_1 and κ_2 which are denoted by $\hat{\kappa}_1$ and $\hat{\kappa}_2$, respectively. The auto-correlation matrix $\tilde{\mathbf{R}}_{\text{s,c}}$ (18) can be formed using those estimates. After that MUSIC algorithm can be readily applied.[1]

When $a_n = 0$ for $n \neq 1$, the estimation procedure of κ_1 and κ_2 changes as given in the following lemma:

Lemma 2: For Case $\Omega_{1,2}$ (i.e., when $a_n = 0$ for $n = 2$), the phase parameters $\{\kappa_i\}_{i=1}^2$ satisfy

$$\kappa_1 = \frac{1}{2}\angle\{-x_1(m)x_3^*(m)\},$$

and

$$\kappa_2 = \angle\{-x_1(m)x_4^*(m)\} - \kappa_1.$$

[1]Note that an auto-correlation matrix of size 4×4 can be formed by padding $e^{j\hat{\kappa}_1}$ at the top of the newly estimated steering vector $\tilde{\mathbf{s}}_{\text{t,c}}$. However, this padding will add complexity to the MUSIC algorithm.

For Case $\Omega_{1,3}$ (i.e., when $a_n = 0$ at $n = 3$), the phase parameters $\{\kappa_i\}_{i=1}^2$ satisfiy

$$\kappa_2 = \frac{1}{2}\angle\{-x_2(m)x_4^*(m)\},$$

and

$$\kappa_1 = \angle\{x_1(m)x_2^*(m)\} + \kappa_2.$$

For Case $\Omega_{1,4}$ (i.e., when $a_n = 0$ at $n = 4$), the phase parameters $\{\kappa_i\}_{i=1}^2$ satisfy

$$\kappa_1 = \frac{1}{2}\angle\{x_1(m)x_3^*(m)\},$$

and

$$\kappa_2 = \angle\{x_2(m)x_1^*(m)\} + \kappa_1.$$

2) CASE 2

Now, we consider the case where $a_n \neq 0$ for all n, i.e., Ω_2. The contribution of the target in the received signal (6) at the m^{th} sample is

$$\mathbf{x}(m) = \mathbf{s}_{\text{t}}s(m), \tag{20}$$

where the joint contribution of the steering vector and the polarization parameters is embedded in

$$\mathbf{s}_{\text{t}} = \begin{bmatrix} e_x e^{j\kappa_1} \\ \frac{1}{\sqrt{2}}(e_x + e_y)e^{j\kappa_2} \\ e_y e^{-j\kappa_1} \\ \frac{1}{\sqrt{2}}(-e_x + e_y)e^{-j\kappa_2} \end{bmatrix}. \tag{21}$$

We want the above vector $\mathbf{s}_{\text{t}}$ to be free from terms e_x and e_y as follows:

$$\mathbf{s}_{\text{t,c}} = \begin{bmatrix} e^{j\kappa_1} \\ e^{j\kappa_2} \\ e^{-j\kappa_1} \\ e^{-j\kappa_2} \end{bmatrix}. \tag{22}$$

Using (21), it can be shown that unlike Case 1, the auto-correlation matrix of $\mathbf{x}(m)$ is a joint function of e_x and e_y and the implementation of Method 1, in this case, requires the knowledge of their ratio. This fact makes Method 1 very difficult to implement for Case 2, whereas, the principle of implementation of Method 2 remains unchanged. Similar to Case 1, Method 2 operates estimating $\{\kappa_i\}_{i=1}^2$. However, the estimation technique is different now, since the received signal vector $\mathbf{x}(m)$ in (20) is different than that in Case 1. After estimating $\{\kappa_i\}_{i=1}^2$, a clean steering vector $\mathbf{s}_{\text{t,c}}$ will be formed (22). The non-signal subspace of its auto-correlation matrix will be used for C-MUSIC.

To estimate $\{\kappa_i\}_{i=1}^2$, we need the following two lemmas.

Lemma 3: If

$$c_1(m) = x_1(m)x_2^*(m) + x_3^*(m)x_4(m),$$

where $x_i(m)$ is the i^{th} element of $\mathbf{x}(m)$ (20), then

$$\angle c_1(m) = \kappa_1 - \kappa_2. \tag{23}$$

Proof: Equation (20) yields

$$x_1(m)x_2^*(m) = \frac{1}{\sqrt{2}}\left(|e_x|^2 + e_x e_y^*\right) e^{j(\kappa_1-\kappa_2)}\sigma_{s,m}^2,$$

and

$$x_3^*(m)x_4(m) = \frac{1}{\sqrt{2}}\left(-e_x e_y^* + |e_y|^2\right) e^{j(\kappa_1-\kappa_2)}\sigma_{s,m}^2.$$

Now we add the above two equations to prove the lemma. ■

Lemma 4: If

$$c_2(m) = -x_1(m)x_4^*(m) + x_3^*(m)x_2(m),$$

then

$$\angle c_2(m) = \kappa_1 + \kappa_2. \tag{24}$$

The proof of the above lemma is similar to that of Lemma 3 and is omitted. The above two lemmas straightforwardly yield the estimates of κ_1 and κ_2 for each sample m. After processing M samples, the auto-correlation matrix for the steering vector $\mathbf{s}_{t,c}$ can be formed to implement MUSIC.[2] Now, we will show how the CF algorithm will be implemented using the estimates of κ_1 and κ_2.

B. CF

Recall that

$$\kappa_1 = \kappa\cos\phi; \quad \kappa_2 = \kappa\sin\phi;$$

and

$$\kappa = \sqrt{\kappa_1^2 + \kappa_2^2} = 2\pi r\sin\theta/\lambda. \tag{25}$$

While performing the CF algorithm, the values of κ_1 and κ_2 are obtained using Lemma 1-2 for Case 1, and Lemma 3-4 for Case 2. In (25), parameter $\kappa = 0$ or $\kappa \neq 0$.

1) When $\kappa = 0$, the elevation angle $\theta = 0°$ indicating that the target is along the $z-$axis and the azimuthal angle has no significance.
2) When $\kappa \neq 0$, parameter κ_1 and κ_2 can't be simultaneously zero due to the elevation angle $0 < \theta \leq 90°$ in (25). The above 3 expressions will be used to estimate the DOA angles in a closed-form manner considering the following 3 combinations of the estimated κ_1 and κ_2.
   a) If $\kappa_1 \neq 0$ and $\kappa_2 \neq 0$, we estimate the azimuthal angle

$$\phi = \arctan\{\kappa_2/\kappa_1\},$$

and since $\kappa > 0$, the sign of κ_1 or κ_2 will help to estimate ϕ without ambiguity. We now use (25) to estimate of the elevation angle as

$$\theta = \arcsin\left(\kappa\lambda/2\pi r\right).$$

   b) If $\kappa_1 = 0$ and $\kappa_2 \neq 0$, the estimate of the azimuthal angle is either 90° (for $\kappa_2 > 0$) or 270° (for $\kappa_2 < 0$). The estimate of term κ is $|\kappa_2|$ which yields the estimate of the elevation angle as

$$\theta = \arcsin\left(|\kappa_2|\lambda/2\pi r\right).$$

   c) If $\kappa_1 \neq 0$ and $\kappa_2 = 0$, the estimate of the azimuthal angle is either 0° (for $\kappa_1 > 0$) or 180° (for $\kappa_1 < 0$). The estimate of term κ is $|\kappa_1|$ which yields the estimate of the elevation angle as

$$\theta = \arcsin\left(|\kappa_1|\lambda/2\pi r\right).$$

Based on the above discussion, the CF algorithm is summarized in Table 1.

TABLE 1. CF algorithm.

κ	$\kappa_1 = \kappa\cos\phi$ $\kappa_2 = \kappa\sin\phi$	Elevation angle (θ)	Azimuthal angle (ϕ)
$\kappa = 0$	$\kappa_1 = 0, \kappa_2 = 0$	0°	N/A
$\kappa \neq 0$	$\kappa_1 \neq 0, \kappa_2 \neq 0$	$\arcsin\left(\kappa\lambda/2\pi r\right)$	$\arctan\{\kappa_2/\kappa_1\}$
			$\kappa_1 > 0, \kappa_2 > 0$ $0° < \phi < 90°$
			$\kappa_1 < 0, \kappa_2 > 0$ $90° < \phi < 180°$
			$\kappa_1 < 0, \kappa_2 < 0$ $180° < \phi < 270°$
			$\kappa_1 > 0, \kappa_2 < 0$ $270° < \phi < 360°$
	$\kappa_1 = 0, \kappa_2 \neq 0$	$\arcsin\left(\kappa_2\lambda/2\pi r\right)$	90° ($\kappa_2 > 0$) or 270° ($\kappa_2 < 0$)
	$\kappa_1 \neq 0, \kappa_2 = 0$	$\arcsin\left(\kappa_1\lambda/2\pi r\right)$	0° ($\kappa_1 > 0$) 180° ($\kappa_1 < 0$)

C. C-MUSIC AND CF WITH $N \geq 4$ ANTENNA ELEMENTS

To keep the computational complexity low, the minimum number of antennas ($N = 4$) is considered in while developing C-MUSIC and CF. Depending on the value of $N \geq 4$, below are two methods that elaborate upon how C-MUSIC and CF can be implemented:

1) When N is a multiple of 4: The elements can be integrated into the array in a circular manner as a multiple of 4 with the same scheme depicted in Theorem 1 and Figure 4. Here, the elements are not necessarily to be parallel to each other. Thus, the circular array can be viewed as b sub-UCAs, where $N = 4b$ and $b = 1, 2, \ldots$ C-MUSIC and CF can then be applied to estimate the DOAs.
   For example, let us consider a circular array with the number of elements, $N = 8$ where the alignment angle of the elements, $\zeta_n = 180°(n-1)/N; n = 1, 2, \ldots, 8$. Hence, the circular array provides two sets of the above sub-UCAs ($b = 2$); one sub-UCA consists of element 1, 3, 5 and 7, and the other one comprises of

[2]To estimate both the DOA angles, we need at least a steering vector of length 3. Therefore an auto-correlation matrix of size 3×3 can be formed by ignoring one of the elements of the newly estimated steering vector $\mathbf{s}_{t,c}$ and it will save some computational complexity.

element 2, 4, 6, and 8. Now, for Case 1, while implementing C-MUSIC using Method 1, we find $\mathbf{F}_n$ similar to Theorem 2 and apply MUSIC to estimate the DOAs. For instance, if antenna 1 gets zero received signal power (i.e.,$\Omega_{1,1}$), we form the auto-correlation matrix of the received signals using other seven elements and multiply that matrix with

$$\mathbf{F_1} = \text{diag}[1/\sin(\zeta_2) \quad 1/\sin(\zeta_3) \quad \dots \quad 1/\sin(\zeta_8)],$$

to clean the non-signal subspace. Now, we are ready to apply MUSIC to estimate the DOAs. While implementing C-MUSIC using Method 2, we estimate the steering elements corresponding to the sub-UCAs using Lemma 1-2 for Case 1, and Lemma 3-4 for Case 2. Thus, we have steering elements, $\{\kappa_i\}_{i=1}^{8}$. Now, we form an 8×8 auto-correlation matrix with the estimated steering elements, and apply MUSIC to estimate the DOAs. As for the CF, we can estimate the DOAs from each sub-UCA separately using Table 1, and finally, average those to increase the estimation accuracy.

2) When N is not a multiple of 4: In this case, we can integrate the elements as the maximum number of 4 element sub-UCAs described above, and the remaining elements as parallel to different elements of those sub-UCAs anywhere on the circumference of the circle. The steering terms of these elements can then be estimated and used to obtain the DOAs.

For example, let us assume the number of antenna elements, $N = 10$. In this case, first, we will design a circular array of $N = 8$ as described earlier with two sub-UCAs. Then the two remaining elements will be placed anywhere on the circumference of the circle in parallel to any of the two elements in those sub-UCAs. We call these elements 9 and 10, and consider they are parallel to element 1 and 2, respectively. This will ensure the same polarization contribution to elements 1 and 9 as well as elements 2 and 10. After estimating the steering elements of 1 and 2 as described in the paper, the steering elements of 9 and 10 can be estimated as

$$\hat{\kappa}_9 = \angle(x_1' * x_9) + \hat{\kappa}_1; \quad \hat{\kappa}_{10} = \angle(x_2' * x_{10}) + \hat{\kappa}_2.$$

Now, similar to our previous discussion, C-MUSIC using Method 1 and 2 and can be applied considering two extra elements. As for the CF, the DOAs are estimated using only the sub-UCAs and averaged to increase the accuracy.

V. IMPLEMENTATION OF THE ALGORITHMS AND ANALYSIS

In the above section, the working principles of the C-MUSIC and CF algorithms were described using the following two assumptions:

1) **Assumption 1:** The system is noise free (i.e., $\sigma = 0$).
2) **Assumption 2:** Due to the contribution of the signal polarization, under the proposed antenna element alignment only one antenna element could suffer in terms of zero RSP and that antenna element is known.

As said, now we want to make the desired algorithms practically realizable. As a result, we first relax Assumption 1 by introducing background noise in the system with known average noise power $\sigma^2 > 0$. However, for an unknown noisy environment, this power can be easily estimated [55], [56]. To relax Assumption 2, we bring in a decision threshold K to check whether the received power at antenna n is below or above this threshold. In particular, after receiving M samples of the received signal $x_n(m)$, the RSP at the antenna element n can be estimated as

$$P_n = \frac{1}{M}\sum_{m=1}^{M} |x_n(m)|^2. \tag{26}$$

In the presence of a target, if $P_n < K$, we decide in the favor of the hypothesis

- H_0: signal is not present at antenna element n due to the compound steering element $a_n = 0$ in (4),

otherwise, we conclude the hypothesis

- H_1: signal is present at antenna element n, and the compound steering element $a_n \neq 0$.

Note that in low average SNR ratio (i.e., $\frac{|a_n|^2}{M}\sum_{m=1}^{M} \sigma_{s,m}^2/\sigma^2$) scenarios, RSP tests at multiple antennas may favor hypothesis H_0 for more than one antenna. If that is the case, our proposed antenna element alignment in Figure 4 dictates us to discard the antenna output with the lowest measured RSP. Our analysis will shortly reveal that such a scenario occurs with negligible probability within the desired operating regime of average SNR.

Now, we discuss how to find the decision threshold K. A popular way of designing the threshold K is based on the Neyman-Pearson lemma. Usually, a prefixed significance level α is set (e.g., $\alpha = 0.001$) to restrict the probability of making a Type I error [i.e., $1 - \text{P}\left(H_0|\Omega_{1,n}\right)$] to a certain percentage (in this case, 0.1%). Next, a test is chosen to minimize Type II error [i.e., $1 - \text{P}\left(H_1|a_n \neq 0\right)$]. Due to the monotonic nature of Type II error w.r.t. K, the value of K will be determined by solving $\text{P}\left(H_0|\Omega_{1,n}\right) = 1 - \alpha$. Next, we present the derivation of $\text{P}\left(H_0|\Omega_{1,n}\right)$.

A. FINDING THRESHOLD K

We propose two different techniques to derive $\text{P}\left(H_0|\Omega_{1,n}\right)$ in order to find K. The first technique, namely Technique 1, is based on the probability density function (PDF) of P_n and the second technique, namely Technique 2, applies the central limit theorem (CLT) to (26) and models P_n as a Gaussian random variable. Now, we elaborate upon Technique 1.

1) TECHNIQUE 1

Given $\Omega_{1,n}$, the received signal samples only contain noise. As a result, $|x_n(m)|^2$ in (26) is a sum of two squared independent identically distributed (i.i.d.) Gaussian random variables each of which has a mean of 0 and a variance of $\sigma^2/2$.

Thus, $|x_n(m)|^2$ is a central chi-square random variable with degrees of freedom (DoF) $= 2$. As the received power P_n in (26) is the average of $|x_n(m)|^2$ for M samples, it also follows a central chi-square distribution with DoF $= 2M$. The probability density function (PDF) of a central chi-square random variable with DoF $= \nu$ is [57]

$$f_\nu(w) = \begin{cases} 0 & w \le 0, \\ \dfrac{w^{\frac{\nu}{2}-1}e^{-\frac{w}{2}}}{2^{\frac{\nu}{2}}\Gamma(\frac{\nu}{2})} & w > 0, \end{cases} \tag{27}$$

and the corresponding cumulative distribution function (CDF) is

$$F_\nu(u) = \int_0^u f_\nu(w)\,dw = \begin{cases} 0 & u \le 0, \\ \dfrac{\Gamma_u(\frac{\nu}{2}, \frac{u}{2})}{\Gamma(\frac{\nu}{2})} & u > 0, \end{cases} \tag{28}$$

where $\Gamma(\frac{\nu}{2}) = \int_0^\infty t^{(\frac{\nu}{2}-1)}e^{-t}dt$ denotes the gamma function, and $\Gamma_u(\frac{\nu}{2}, \frac{u}{2}) = \int_0^{\frac{u}{2}} t^{(\frac{\nu}{2}-1)}e^{-t}\,dt$ represents the lower incomplete gamma function. Now, we use (27) to write the conditional PDF of the measured power P_n given Case $\Omega_{1,n}$ as

$$f_{P_n|\Omega_{1,n}}(w) = \frac{1}{\tilde{\sigma}^2} f_\nu\left(\frac{w}{\tilde{\sigma}^2}\right), \tag{29}$$

where $\tilde{\sigma}^2 = \sigma^2/2M$. Our goal was to find $\mathrm{P}\left(H_0|\Omega_{1,n}\right) = \mathrm{P}\left(P_n \le K|\Omega_{1,n}\right)$, which is

$$\int_0^K f_{P_n|\Omega_{1,n}}(w)\,dw = \int_0^K \frac{1}{\tilde{\sigma}^2} f_\nu\left(\frac{w}{\tilde{\sigma}^2}\right) dw = F_\nu\left(\frac{K}{\tilde{\sigma}^2}\right), \tag{30}$$

where the last equality is obtained from (28). Now, we numerically solve $F_\nu\left(\frac{K}{\tilde{\sigma}^2}\right) = 1 - \alpha$ to find the decision threshold K. For fixed M and σ^2, the value of K can be precomputed. However, this method could be computationally complex and time-consuming especially for a time-varying noise environment. That environment may demand a quick method and the following technique (i.e., Technique 2) could be found more useful.

2) TECHNIQUE 2

To obtain a quick value of K, we apply CLT to (26). The chi-square distribution given in (29) yields the conditional mean of P_n as $\mu_{P_n|\Omega_{1,n}} = \sigma^2$, and its variance $\sigma^2_{P_n|\Omega_{1,n}} = \sigma^4/M$. The desired probability $\mathrm{P}\left(H_0|\Omega_{1,n}\right) = \mathrm{P}\left(P_n \le K|\Omega_{1,n}\right)$ which is

$$\mathrm{P}\left(H_0|\Omega_{1,n}\right) = 1 - \mathrm{P}\left(P_n > K|\Omega_{1,n}\right),$$

and under CLT, it simplifies to

$$\mathrm{P}\left(H_0|\Omega_{1,n}\right) = 1 - Q\left(\frac{M\left(K - \sigma^2\right)}{\sigma^4}\right),$$

where $Q(\cdot)$ is the tail distribution function of the standard normal distribution. Now, we solve $Q\left(\frac{M(K-\sigma^2)}{\sigma^4}\right) = \alpha$ to get the value of K.

B. ANALYSIS

Recall that in a noiseless polarized sensitive environment, under the proposed antenna element assignment scheme two cases can occur; Case 1 ($a_n = 0$, where $n = 1$ or 2 or 3 or 4), and Case 2 ($a_n \neq 0$ for all n). Both C-MUSIC and CF operate differently in each of the above cases. Therefore, the performance of the algorithms will depend on how accurately those cases can be identified after processing M samples of the received signal. Our next objective is to analyze $\mathrm{P}\left(I|\Omega_i\right)$, which is the probability of accurately identifying Case i given Case i occurred for a given set of source parameters, where $i = 1, 2$. Since Case 1 has 4 sub-cases, and $\mathrm{P}\left(I|\Omega_1\right)$ is different for each of those sub-cases, we need to add another condition (i.e., $a_n = 0$) in the derivation of the desired probability. Thus, for Case 1, we analyze $\mathrm{P}\left(I|\Omega_{1,n}\right)$. In the derivation of the desired probability for Case 1, we will exploit the following two lemmas. The 1st one is straightforwardly obtained from (28).

Lemma 5: Given Case 1 due to $a_n = 0$ (i.e., $\Omega_{1,n}$), the conditional probability of the measured received power at antenna n (i.e., P_n) below the decision threshold K is

$$\mathrm{P}\left(P_n \le K|\Omega_{1,n}\right) = F_\nu\left(\frac{K}{\tilde{\sigma}^2}\right). \tag{31}$$

Given Case $\Omega_{1,n}$, the conditional PDF of the measured received power at antenna $n' \neq n$ follows a non-central chi-square distribution defined as [58] and [59]

$$f_{P_{n'}|\Omega_{1,n}}(w) = \frac{1}{\tilde{\sigma}^2} f_{\nu,\,n'}\left(\frac{w}{\tilde{\sigma}^2}\right), \tag{32}$$

where

$$f_{\nu,\,n'}(w) = \begin{cases} \exp\left(-\dfrac{\Delta_{n'}}{2}\right) \sum_{j=0}^{+\infty} \dfrac{\Delta_{n'}^j}{2^j j!} f_{2j+\nu}(w) & w > 0, \\ 0 & \text{otherwise.} \end{cases} \tag{33}$$

In (33), $\Delta_{n'} = \sum_{m=1}^{M} 2\mu^2_{m,\,n'}/\sigma^2$ is the non-centrality parameter where $\mu^2_{m,\,n'} = |a_{n'}|^2\sigma^2_{s,m}$ at the n'^{th} element, and $f_{2j+\nu}(w)$ follows the central chi-square distribution (27) with DoF $= 2j + \nu$. Integrating both sides of (33) from K to ∞, we get

$$\bar{F}_{\nu,\,n'}(K) = \exp\left(-\frac{\Delta_{n'}}{2}\right) \sum_{j=0}^{+\infty} \frac{\Delta_{n'}^j}{2^j j!} \bar{F}_{2j+\nu}(K), \tag{34}$$

where $\bar{F}_{2j+\nu}(K) = 1 - F_{2j+\nu}(K)$ is the complement of the CDF given in (28). Now, we are ready to state the other lemma to get the desired probability $\mathrm{P}\left(I|\Omega_{1,n}\right)$.

Lemma 6: Given Case 1 due to $a_n = 0$ (i.e., $\Omega_{1,n}$), the conditional probability of the received measured power at antenna $n' \neq n$ (i.e., $P_{n'}$) above the decision threshold K is

$$\mathrm{P}\left(P_{n'} > K|\Omega_{1,n}\right) = \bar{F}_{\nu,\,n'}\left(\frac{K}{\tilde{\sigma}^2}\right). \tag{35}$$

Since the received noise vector at antenna n is independent of that at antenna $n' \neq n$, we get the desired conditional probability $\mathrm{P}\left(I|\Omega_{1,n}\right)$ as stated in the following theorem.

Theorem 3: Given Case 1 due to $a_n = 0$ (i.e. $\Omega_{1,n}$), the conditional probability of accurately identifying Case 1 is

$$\begin{aligned}\mathrm{P}\left(I|\Omega_{1,n}\right) &= \mathrm{P}\left(P_n \leq K|\Omega_{1,n}\right) \\ &\quad \times \prod_{n'=1,\neq n}^{4} \mathrm{P}\left(P_{n'} > K|\Omega_{1,n}\right) \\ &= F_{\nu}\left(\frac{K}{\tilde{\sigma}^2}\right) \prod_{n'=1,\neq n}^{4} \bar{F}_{\nu,n'}\left(\frac{K}{\tilde{\sigma}^2}\right).\end{aligned}$$

The Reader must note that the probability in Theorem 3 will change from one sub-case to another in Case 1. However, since $\bar{F}_{\nu,n'}\left(\frac{K}{\tilde{\sigma}^2}\right) \leq 1$ and $F_{\nu}\left(\frac{K}{\tilde{\sigma}^2}\right) = 1-\alpha$, the probability in Theorem 3 will have the same upper bound for all n as given in the following corollary.

Corollary 1: Given Case 1 due to $a_n = 0$ (i.e. $\Omega_{1,n}$), the conditional probability of accurately identifying Case 1 is upper bounded by

$$\mathrm{P}\left(I|\Omega_{1,n}\right) \leq 1-\alpha; \quad \forall n.$$

In Case 2, $a_n \neq 0$ $\forall n$, and the conditional PDF of the measured received power $f_{P_n|\Omega_2}(w)$ follows a non-central chi-square distribution similar to (32). This distribution coupling with the fact that the received noise vector at antenna n is independent of that at antenna $n' \neq n$ gives us the following theorem.

Theorem 4: Given Case 2 (i.e., Ω_2), the conditional probability of accurately identifying Case 2 is

$$\mathrm{P}\left(I|\Omega_2\right) = \prod_{n=1}^{4} \mathrm{P}\left(P_n > K|\Omega_2\right) = \bar{F}_{\nu,n}\left(\frac{K}{\tilde{\sigma}^2}\right).$$

VI. NUMERICAL RESULTS

In this section, our objectives are 1) to provide insights into the system performance through numerical examples based on our analytical results, and 2) to perform a thorough comparative study between C-MUSIC and CF algorithms. In all numerical examples, i) a 4-element UCA is considered with the antenna alignment scheme shown in Figure 4, ii) the number of samples $M = 50$, iii) the significance level $\alpha = 0.001$, iv) received waveform samples modelled as i.i.d. complex Gaussian random variables with mean = 0 and variance = 1/2 per dimension, unless otherwise specified.

Recall that identification of each of the five effective cases is performed employing the decision threshold K obtained from the analysis. It can be determined by setting Type I Error (i.e., $1-\mathrm{P}\left(H_0|\Omega_{1,n}\right)$) equals to α using either Technique 1 or Technique 2. In Figure 6, the decision threshold normalized by the average noise power is plotted by setting $\alpha = 0.001$. Here, it can be noticed that Technique 1 (which is based on the exact PDF of the decision statistics) yields a slightly higher value of K than Technique 2 (which is based on the CLT). This higher value of K will result in higher Type II error and its effects will be demonstrated shortly.

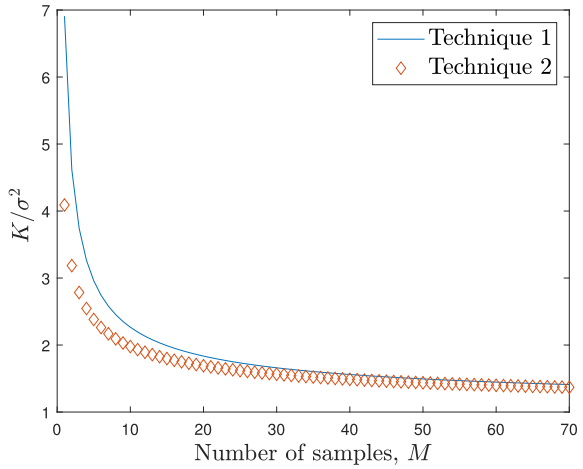

FIGURE 6. Normalized threshold K vs number of samples M.

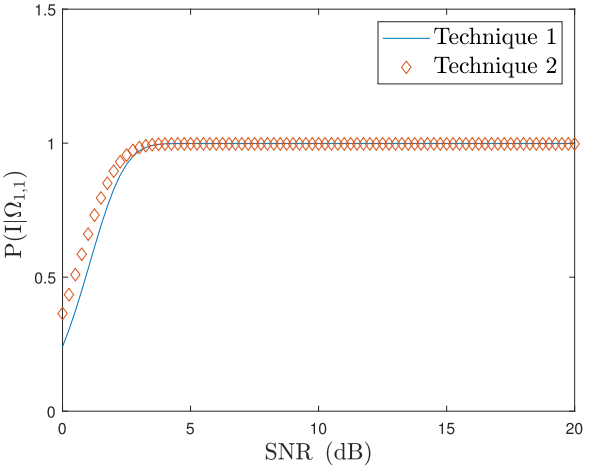

FIGURE 7. Probability of correctly identifying Case 1.

In the next example, we evaluate our derived expression of $\mathrm{P}\left(I|\Omega_{1,n}\right)$ (i.e., the conditional probability of accurately identifying Case 1) given in Theorem 3 as a function of average (received) SNR using both Technique 1 and Technique 2; see Figure 7. Here, Case 1 occurs due to the DOA angles $\phi = 30°$, $\theta = 70.529°$, and polarization parameters $\eta = 0°$, $\gamma = 60°$. These parameters cause $a_n = 0$ at $n = 1$. In Figure 7, it can be noticed that Technique 2 slightly performs better than Technique 1 especially at low average SNR due to the use of a higher value of K. We also see that when the average SNR is above or equal to 4 dB, both techniques exhibit the maximum achievable performance as implied by Corollary 1. In Figure 8, we plot $\mathrm{P}\left(I|\Omega_2\right)$ (i.e. the conditional probability of accurately identifying Case 2) given in Theorem 4 as a function of average SNR for both Technique 1 and Technique 2. Here, the DOA and polarization parameters are $\phi = 45°$, $\theta = 10°$, $\eta = 90°$ and $\gamma = 45°$, respectively. Similar to

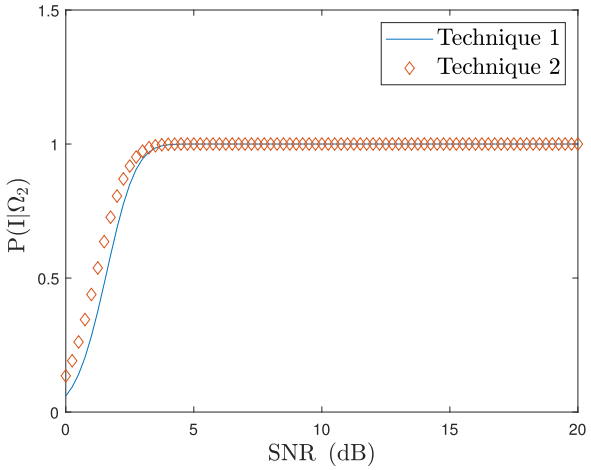

FIGURE 8. Probability of correctly identifying Case 2.

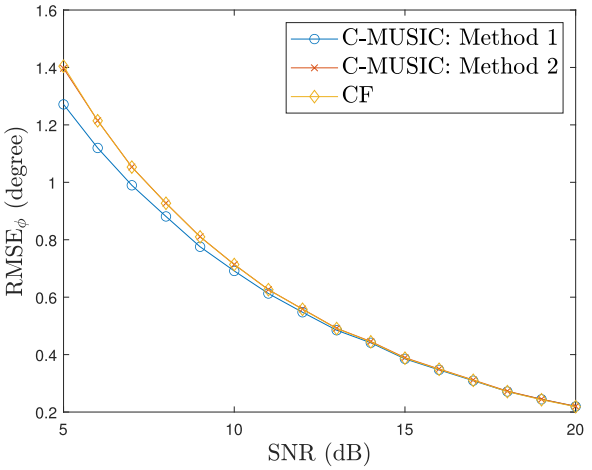

FIGURE 9. $RMSE_\phi$ vs average (received) SNR for Case 1.

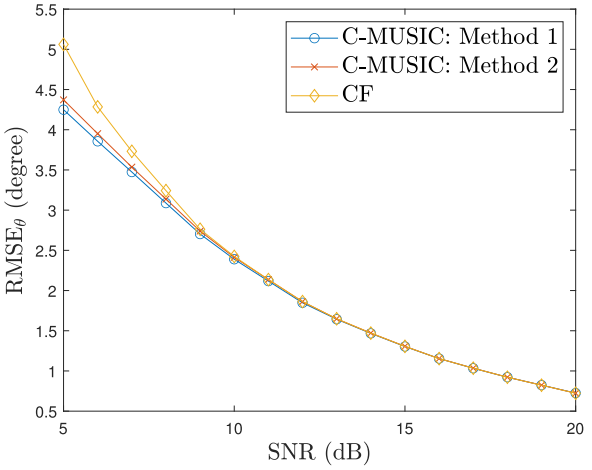

FIGURE 10. $RMSE_\theta$ vs average (received) SNR for Case 1.

Figure 7, the results in Figure 8 suggest that both techniques are equally capable of identifying Case 2 almost perfectly when the average SNR $\geq$ 4 dB. From now on, Technique 2 will be employed to design the decision threshold K.

Next, we would like to compare the performance of the CF algorithm against that of the C-MUSIC for Case 1 and Case 2. As explained in Section III, the conventional MUSIC fails to yield reliable DOA estimates in Case 1, however, in Case 2, it can operate by placing all the antenna elements in the same direction. Therefore, in our simulation for the latter case, the conventional MUSIC is used as the baseline algorithm assuming no contribution from the polarization (i.e., $e_n = 1$ in (2) for all n). Let us first consider Case 1 due to $a_1 = 0$ (i.e., $\Omega_{1,1}$), where $\phi = 30°$, $\theta = 70.529°$, $\eta = 0°$ and $\gamma = 60°$; see Figure 9 and 10, where RMSE (Root Mean Square Error) is plotted as a function of the average SNR. C-MUSIC has been implemented using both Method 1 and Method 2 where the former is observed to exhibit slightly better performance than the latter. Here, it can also be noticed that as expected, at a low average SNR (close to 5 dB) the performance difference between C-MUSIC and CF algorithms is somewhat noticeable. However, as the average SNR increases that performance difference starts to diminish. At average SNR $\geq$ 10 dB, both CF and C-MUSIC algorithms exhibit almost identical performance. Similar observations are made in Case 2 for $\phi = 45°$, $\theta = 10°$, $\eta = 90°$ and $\gamma = 45°$; see Figure 11 and 12, where the RMSEs of C-MUSIC and CF algorithms are compared against that of the polarization contamination free MUSIC. As expected, the latter algorithm exhibits slightly superior performance compared to the former two algorithms. However, the performance difference diminishes with the increase in SNR. It is interesting to notice that, the RMSE on the elevation plane is greater than that on the azimuthal plane for Figure 9 and 10, and the opposite is observed in Figure 11 and 12. Depending on SNR and the number of samples, the RMSE of the estimation depends on the contributions of the DOA and polarization angles to the signal space. In a special situation, when the contributions of both the DOA angles are the same (e.g. $\theta = \phi = 45°$, where the sine and cosine terms are identical), the above RMSE difference diminishes.

In the following numerical study, we would like to demonstrate the performance of both the algorithms as the system transits from one case to another due to the change in the azimuthal angle. Please see Figure 13, and 14, where we plot RMSE by varying the azimuth angle ϕ (with the increment of $\pm 0.5°$). Here, we use average SNR = 20 dB, $\theta = 70.529°$, $\eta = 0°$ and $\gamma = 60°$. Note that when $\phi = 30°$, Case 1 occurs due to $a_1 = 0$ and otherwise, we have Case 2. Using the above two figures, we make the following set of observations: 1) the designed decision threshold K is capable of efficiently differentiating between Case 1 and Case 2, 2) the RMSE of Case 2 is slightly higher than Case 1 since as ϕ approaches 30°, compound steering element a_1 approaches 0. Thus, it is better to discard the output of antenna element 1, 3) as expected, Case 1 occurs for two different azimuthal angles which are 180° apart from each other, and 4) both the CF and C-MUSIC algorithms not only exhibit almost identical performance but also robust to the transition from Case 1 to

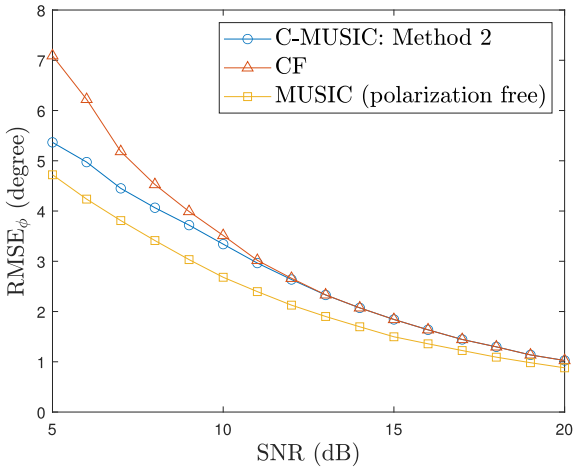

FIGURE 11. ***RMSE$_\phi$*** **vs average (received) SNR for Case 2.**

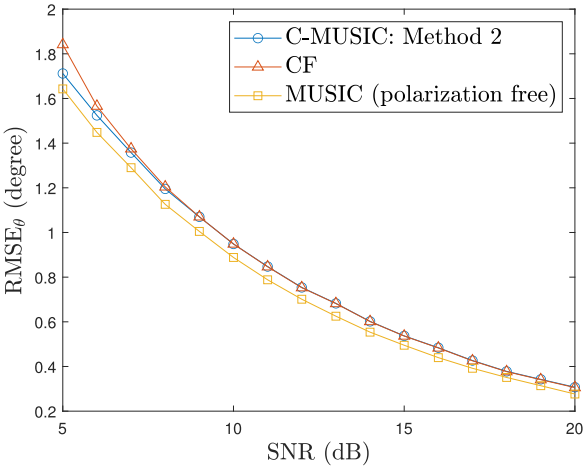

FIGURE 12. ***RMSE$_\theta$*** **vs average (received) SNR for Case 2.**

Case 2 or vice versa. Similar results are also observed when we vary the elevation angles for a given azimuthal angle. For conciseness, figures related to those observations are omitted.

Finally, we compare the complexity of the CF and C-MUSIC algorithms. In our calculation, we consider the complexity incurred after identifying Case i, where $i = 1, 2$. The complexities of the algorithms are measured by the number of real-time multiplications associated with the major operations. Note that one complex multiplication is equivalent to four real multiplications. In C-MUSIC: Method 1 (only applicable for Case 1), a new matrix is formed which requires $4(N-1)^2M + 2(N-1)^2 - (N-1) + 2(N-1)^2 - (N-1)$ real multiplications, where N represents the number of antenna elements and M denotes the number of samples. Here, $4(N-1)^2M + 2(N-1)^2 - (N-1)$ is due to the estimation of the auto-correlation matrix and the additional $2(N-1)^2 - (N-1)$ is an upper bound on the number of multiplications between the auto-correlation matrix and the diagonal matrix $\mathbf{F}_n$; $n = 1, 2, 3, 4$. As previously discussed, both C-MUSIC (Method 2) and CF operate by estimating the phases of the steering elements, κ_1, and κ_2. The cost

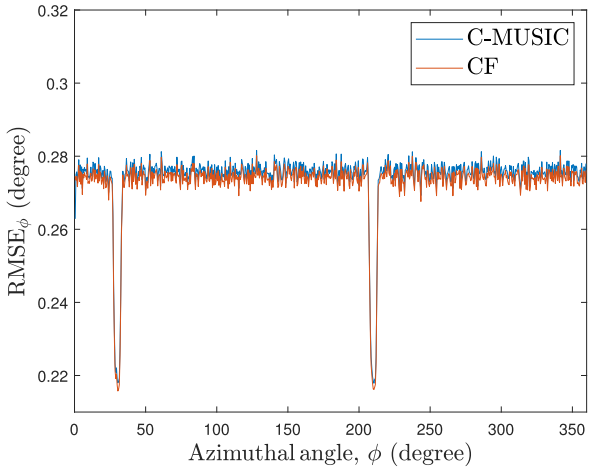

FIGURE 13. ***RMSE$_\phi$*** **as a function of the azimuthal angle ϕ.**

TABLE 2. Complexity analysis.

Algorithm		Case 1	Case 2
C-MUSIC	Method 1	$(N-1)^2(4M+4)$ $-2(N-1)$ $+12(N-1)^3$ $+N_\theta N_\phi \times$ $\{4N^2-10N+5\}$	N/A
	Method 2	$8M+2\log_2 p+1$ $+12(N-1)^3$ $+N_\theta N_\phi \times$ $\{4N^2-10N+5\}$	$16M+2\log_2 p+1$ $+12N^3$ $+N_\theta N_\phi \times$ $\{4N^2-2N-1\}$
CF		$8M+6$ $+4\log_2 p$	$16M+6$ $+4\log_2 p$

associated with this estimation is $8M + 2\log_2 p + 1$ real multiplications for Case 1, and $16M + 2\log_2 p + 1$ real multiplications for Case 2, where p refers to the number of digits of precision [60], [61]. It is known that the MUSIC algorithm performs eigenvalue decomposition (EVD) which often is obtained from a singular value decomposition (SVD). As per [62], this complexity associated with an SVD is $12N^3$. As C-MUSIC (Method 1 and 2) operates on the 2D MUSIC algorithm, the DOA angle search using the null space requires $12N^3 + N_\theta N_\phi\{4N(N-1)+2(N-1)+1\}$ real multiplications, where N_θ and N_ϕ represent the searching point number on the azimuthal and elevation planes, respectively. On the other hand, the required cost to estimate the DOA angles is upper bounded by $1 + \log_2 p + 3 + 1 + \log_2 p$ from the estimates of κ_1, and κ_2 using the CF algorithm. Here, the first two terms are related to the estimation of the azimuthal angle ϕ, the third term is to calculate the κ, and the rest of the terms are associated with the estimation of the elevation angle θ. All the corresponding costs are added and tabulated in Table 2 for complexity comparison. According to this table, the cubic order of the array size, the number of samples, and the product of the searching points dominate the complexity of the C-MUSIC algorithm, whereas, the complexity of the CF algorithm is primarily dictated by the number of samples.

Now, we use Table 2 to demonstrate the complexities of the DOA estimating algorithms by using numerical examples. Please see Figure 15, and 16, where the complexities of

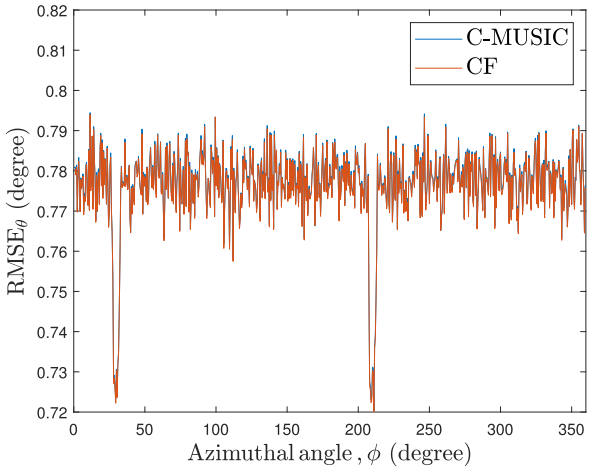

FIGURE 14. *RMSE*$_\theta$ as a function of the azimuthal angle ϕ.

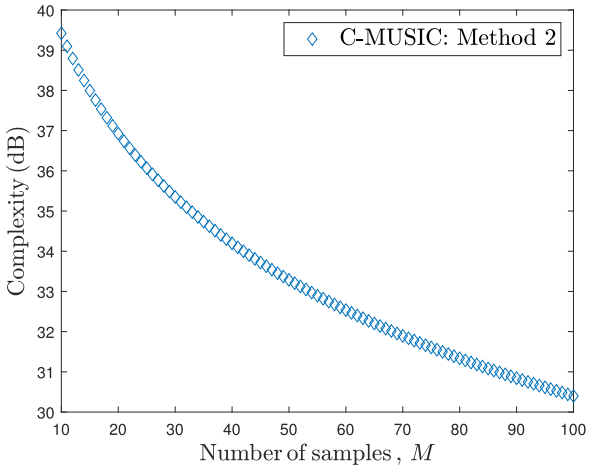

FIGURE 16. Complexity vs number of samples *M* for Case 2.

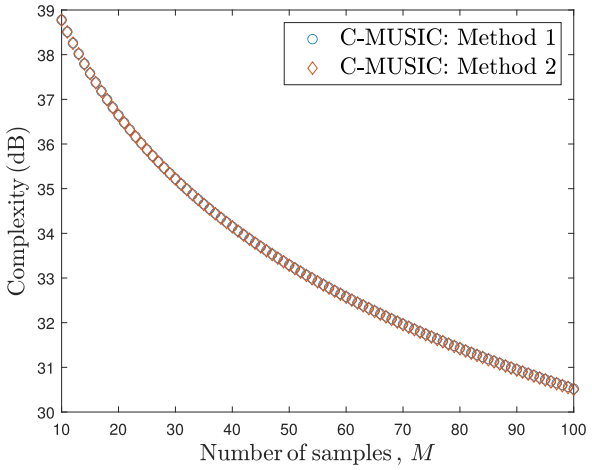

FIGURE 15. Complexity vs number of samples *M* for Case 1.

C-MUSIC (w.r.t the CF algorithm) are plotted as functions of the number of samples M for Case 1 and Case 2, respectively. Here, the search in MUSIC is conducted with 1° precision of the DOA angles. The results in those figures jointly suggest that the CF algorithm offers significant complexity gain over the C-MUSIC. For instance, this gain is over 33 dB in Case 1 (Method 1 and Method 2), and Case 2 (Method 2) for $M = 50$, and $p = 1024$. This gain decreases as the number of samples M increases.

VII. APPLICATIONS AND FUTURE WORKS

As discussed previously, single source 2-D DOA estimation has attracted interest due to its numerous applications [11], [12], [13], [14], [15], [16], [17], [18]. There exist many scenarios where our developed method can be implemented to estimate the DOAs while handling the polarization contamination. One of the most important uses of our developed scheme is in the defense industry (i.e., tracking an airborne target with high precision), where the polarization contamination degrades the performance of DOA estimation. Although the polarization of the transmitter can be previously known, the polarization state of the transmitted signal can change when the electromagnetic wave scatters from a target [41], [42], [43]. Therefore, an arbitrary alignment of the antennas and polarization blind DOA estimation technique may lead to unreliable DOA estimation due to Case 1 as explained in this paper. Another use can be in the field of wireless communication. Since our method uses the minimum number of simple short dipole antennas, it provides area and cost-effectiveness in terms of hardware implementation to tackle the polarization issue. Therefore, it can be used in the user equipment to provide quick and robust DOA estimation. Although our developed C-MUSIC and CF algorithms are shown for a single source DOA application, they can also be directly implemented in multi-user environments, where users are orthogonal in either time, frequency, or code. Recall that we assumed the source signal as unknown and developed a single decision threshold to determine whether Case 1 or 2 occurred. In a U-user non-orthogonal environment, we would require designing multiple decision thresholds for all users. In addition, these thresholds will not only be functions of the noise power but also the parameters of other users, since an antenna captures the sum of all sources' signals. Currently, designing these thresholds and cleansing the steering elements for non-orthogonal users in a multi-user environment remain open challenges and we leave those topics as our future works.

VIII. CONCLUSION

In this paper, we addressed the problem of localizing a single narrowband source in all possible polarization scenarios just employing simple (short dipole) antenna elements and signal processing techniques. Depending on the antenna alignment, the contribution of the polarization and DOA angles could result in poor received signal power at one or more antenna elements. To overcome this issue, an antenna alignment scheme was mathematically developed for a UCA that operates with the minimum number of required antenna elements. Under this scheme, antenna elements are aligned in

such a way that not more than one element will suffer from low received signal power due to the joint effects of polarization and DOA angles. A decision threshold was developed to decide whether the antenna element with the smallest received power should be considered in the process of DOA estimation or not. We demonstrated how the polarization contribution can be suppressed from the non-signal subspace in order for the popular MUSIC algorithm to operate in all the polarization scenarios. During the process of cleaning the non-signal subspace, we designed an algorithm that estimates the DOA angles in a closed-form manner. Of course, the latter is significantly less complex than the former. Our numerical results demonstrated that depending on the system condition, that gain could be more than 33 dB without sacrificing any performance as long as the average (received) SNR is 10 dB or more at number of samples $M = 50$.

REFERENCES

[1] Z. Chen, G. Gokeda, and Y. Yu, *Introduction to Direction-of-Arrival Estimation*. Norwood, MA, USA: Artech House, 2010.
[2] N. R. Council, *Spatial Statistics and Digital Image Analysis*. Washington, DC, USA: National Academies Press, 1991.
[3] M.-J. Zhou, C. Ge, X.-P. Lin, L. He, and X.-F. Zhang, "A DOA tracking algorithm for coprime planar array via PAST," in *Proc. 4th Annu. Int. Conf. Netw. Inf. Syst. Comput. (ICNISC)*, Apr. 2018, pp. 89–95.
[4] J. Liu and X. Liu, "Joint 2-D DOA tracking for multiple moving targets using adaptive frequency estimation," in *Proc. IEEE Int. Conf. Acoust., Speech Signal Process. (ICASSP)*, Apr. 2007, p. 1113.
[5] M. I. Hasan, M. Dautta, and M. A. Haque, "A study of ferromagnetic object detection in ocean environment using empirical mode decomposition," in *Proc. TENCON IEEE Region Conf.*, Nov. 2017, pp. 2132–2135.
[6] F. Mendoza- Montoya, D. H. Covarrubias-Rosales, and C. A. Lopez-Miranda, "DOA estimation in mobile communications system using subspace tracking methods," *IEEE Latin America Trans.*, vol. 6, no. 2, pp. 123–129, Jun. 2008.
[7] A. Abdelbari and B. Bilgehan, "A novel DOA estimation method of several sources for 5G networks," in *Proc. Int. Conf. Electr., Commun., Comput. Eng. (ICECCE)*, Jun. 2020, pp. 1–6.
[8] M. Rzymowski, K. Trzebiatowski, K. Nyka, and L. Kulas, "DoA estimation using reconfigurable antennas in millimiter-wave frequency 5G systems," in *Proc. 17th IEEE Int. New Circuits Syst. Conf. (NEWCAS)*, Jun. 2019, pp. 1–4.
[9] H. Zhou, Y. Liu, C. Lv, Y. Li, and J. Yu, "A beamspace-based DOA estimation algorithm for 2D massive MIMO systems," in *Proc. IEEE 11th Int. Conf. Commun. Softw. Netw. (ICCSN)*, Jun. 2019, pp. 546–552.
[10] M. Burtowy, M. Rzymowski, and L. Kulas, "Low-profile ESPAR antenna for RSS-based DoA estimation in IoT applications," *IEEE Access*, vol. 7, pp. 17403–17411, 2019.
[11] M. Doroslovački and E. G. Larsson, "Nonuniform linear antenna arrays minimising Cramér–Rao bounds for joint estimation of single source range and direction of arrival," *IEE Proc.-Radar, Sonar Navigat.*, vol. 152, no. 4, pp. 225–231, 2005.
[12] D. Ying and Y. Yan, "Robust and fast localization of single speech source using a planar array," *IEEE Signal Process. Lett.*, vol. 20, no. 9, pp. 909–912, Sep. 2013.
[13] H. Lee and R. Stovall, "Maximum likelihood methods for determining the direction of arrival for a single electromagnetic source with unknown polarization," *IEEE Trans. Signal Process.*, vol. 42, no. 2, pp. 474–479, Feb. 1994.
[14] D. Hertz and I. Ziskind, "Fast approximate maximum likelihood algorithm for single source localisation," *IEE Proc. Radar, Sonar Navigat.*, vol. 142, no. 5, pp. 232–235, Oct. 1995.
[15] I. D. Chyrka and I. P. Omelchuk, "Instantaneous DoA estimation for a single source," in *Proc. 17th Int. Radar Symp. (IRS)*, May 2016, pp. 1–4.
[16] L. Zhang, Z. Ye, Y. Zhang, S. Li, J. Li, and W. Jiang, "Underdetermined mixing matrix estimation based on single source detection," in *Proc. China Int. SAR Symp. (CISS)*, Oct. 2018, pp. 1–4.
[17] R. T. Suryaprakash and R. R. Nadakuditi, "Consistency and MSE performance of MUSIC-based DOA of a single source in white noise with randomly missing data," *IEEE Trans. Signal Process.*, vol. 63, no. 18, pp. 4756–4770, Sep. 2015.
[18] M. I. Hasan and M. Saquib, "Low complexity single source 2-D DOA estimation based on reduced dimension SVR," in *Proc. IEEE 22nd Annu. Wireless Microw. Technol. Conf. (WAMICON)*, Apr. 2022, pp. 1–4.
[19] R. O. Schmidt, "Multiple emitter location and signal parameter estimation," *IEEE Trans. Antennas Propag.*, vol. AP-34, no. 3, pp. 276–280, Mar. 1986.
[20] A. G. Jaffer, "Maximum likelihood direction finding of stochastic sources: A separable solution," in *Proc. Int. Conf. Acoust., Speech, Signal Process.*, Jan. 1988, pp. 2893–2894.
[21] J. Capon, "High-resolution frequency-wavenumber spectrum analysis," *Proc. IEEE*, vol. 57, no. 8, pp. 1408–1418, Aug. 1969.
[22] A. Paulraj, R. Roy, and T. Kailath, "A subspace rotation approach to signal parameter estimation," *Proc. IEEE*, vol. 74, no. 7, pp. 1044–1046, Jul. 1986.
[23] R. Kumaresan and D. W. Tufts, "Estimating the angles of arrival of multiple plane waves," *IEEE Trans. Aerosp. Electron. Syst.*, vol. AES-19, no. 1, pp. 134–139, Jan. 1983.
[24] A. Patwari and G. R. Reddy, "1D direction of arrival estimation using root-MUSIC and ESPRIT for dense uniform linear arrays," in *Proc. 2nd IEEE Int. Conf. Recent Trends Electron., Inf. Commun. Technol. (RTEICT)*, May 2017, pp. 667–672.
[25] Y. I. Abramovich, N. K. Spencer, and A. Y. Gorokhov, "DOA estimation for noninteger linear antenna arrays with more uncorrelated sources than sensors," *IEEE Trans. Signal Process.*, vol. 48, no. 4, pp. 943–955, Apr. 2000.
[26] I. A. H. Adam and M. D. R. Islam, "Perfomance study of direction of arrival (DOA) estimation algorithms for linear array antenna," in *Proc. Int. Conf. Signal Process. Syst.*, May 2009, pp. 268–271.
[27] L. Huang and Y. L. Lu, "Multiple sources DOA and polarization estimations using vector circular array," in *Proc. IET Int. Radar Conf.*, 2013, pp. 1–4.
[28] X. Guo, Y. Huang, B. Li, and L. Chu, "DOA estimation of mixed circular and non-circular signals using uniform circular array," in *Proc. 7th Int. Congr. Image Signal Process.*, Oct. 2014, pp. 1043–1047.
[29] M. I. Hasan and M. Saquib, "Performance of large aperture UCCA arrays in a 5G user dense network," 2022, *arXiv:2203.02491*.
[30] Z. Xiaofei, S. Ying, Z. Ruina, L. Wen, and X. Dazhuan, "Blind 2D-DOA estimation for uniform circular array," in *Proc. Int. Symp. Microw., Antenna, Propag. EMC Technol. Wireless Commun.*, Aug. 2007, pp. 589–592.
[31] K. Cui, X. Chen, J. Huang, and N. Yuan, "A novel DOA estimation algorithm for a 5-element circular array," in *Proc. IEEE 2nd Adv. Inf. Technol., Electron. Autom. Control Conf. (IAEAC)*, Mar. 2017, pp. 1224–1228.
[32] S. A. Vorobyov, A. B. Gershman, and Z.-Q. Luo, "Robust adaptive beamforming using worst-case performance optimization: A solution to the signal mismatch problem," *IEEE Trans. Signal Process.*, vol. 51, no. 2, pp. 313–324, Feb. 2003.
[33] J. W. Kim and C. K. Un, "An adaptive array robust to beam pointing error," *IEEE Trans. Signal Process.*, vol. 40, no. 6, pp. 1582–1584, Jun. 1992.
[34] N. K. Jablon, "Adaptive beamforming with the generalized sidelobe canceller in the presence of array imperfections," *IEEE Trans. Antennas Propag.*, vol. AP-34, no. 8, pp. 996–1012, Aug. 1986.
[35] A. B. Gershman, V. I. Turchin, and V. A. Zverev, "Experimental results of localization of moving underwater signal by adaptive beamforming," *IEEE Trans. Signal Process.*, vol. 43, no. 10, pp. 2249–2257, Oct. 1995.
[36] J. Ringelstein, A. B. Gershman, and J. F. Bohme, "Direction finding in random inhomogeneous media in the presence of multiplicative noise," *IEEE Signal Process. Lett.*, vol. 7, no. 10, pp. 269–272, Oct. 2000.
[37] Y. J. Hong, C.-C. Yeh, and D. R. Ucci, "The effect of a finite-distance signal source on a far-field steering Applebaum array-two dimensional array case," *IEEE Trans. Antennas Propag.*, vol. AP-36, no. 4, pp. 468–475, Apr. 1988.
[38] J. Goldberg and H. Messer, "Inherent limitations in the localization of a coherently scattered source," *IEEE Trans. Signal Process.*, vol. 46, no. 12, pp. 3441–3444, Dec. 1998.
[39] O. Besson, A. A. Monakov, and C. Chalus, "Signal waveform estimation in the presence of uncertainties about the steering vector," *IEEE Trans. Signal Process.*, vol. 52, no. 9, pp. 2432–2440, Sep. 2004.

[40] O. Besson and F. Vincent, "Performance analysis of beamformers using generalized loading of the covariance matrix in the presence of random steering vector errors," *IEEE Trans. Signal Process.*, vol. 53, no. 2, pp. 452–459, Feb. 2005.
[41] J. Groot, "Introduction to radar polarimetry," Fysisch En Elektronisch Lab TNO, The Hague, The Netherlands, Tech. Rep. FEL-91-B122, 1991.
[42] E. Bahar, G. Huang, and B. S. Lee, "Electromagnetic scattering and depolarization across rough surfaces: Full wave analysis," *Radio Sci.*, vol. 30, no. 3, pp. 525–544, May 1995.
[43] B. Emery and A. Camps, *Introduction to Satellite Remote Sensing: Atmosphere, Ocean, Land and Cryosphere Applications*. Amsterdam, The Netherlands: Elsevier, 2017.
[44] J. Li and R. T. Compton, Jr., "Angle and polarization estimation using ESPRIT with a polarization sensitive array," *IEEE Trans. Antennas Propag.*, vol. 39, no. 9, pp. 1376–1383, Sep. 1991.
[45] L. Shuai, J. Ming, and Q. Xiaolin, "Joint polarization-DOA estimation using circle array," in *Proc. IET Conf. Publications*, 2009, pp. 1–5.
[46] X. Lan, W. Liu, and H. Y. T. Ngan, "Joint 4-D DOA and polarization estimation based on linear tripole arrays," in *Proc. 22nd Int. Conf. Digit. Signal Process. (DSP)*, Aug. 2017, pp. 1–5.
[47] L. Wang, G. Wang, and Z. Chen, "Joint DOA-polarization estimation based on uniform concentric circular array," *J. Electromagn. Waves Appl.*, vol. 27, no. 13, pp. 1702–1714, Sep. 2013.
[48] J.-C. Huang, Y.-W. Shi, and J.-W. Tao, "Closed-form estimation of DOA and polarization for multisource with a uniform circular array," in *Proc. Int. Conf. Mach. Learn. Cybern.*, vol. 7, Aug. 2005, pp. 4469–4474.
[49] M. Zhang and T. Lyu, "Multi-parameter estimation based on improved MUSIC algorithm for polarization sensitive array," in *Proc. Int. Workshop Electromagn., Appl. Student Innov. Competition (iWEM)*, Sep. 2019, pp. 1–4.
[50] S. Shamrao and B. Suryakanth, "A survey on design and development of planar antennas for wireless applications," *Int. J. Emerg. Technol.*, vol. 6, no. 2, p. 203, 2015.
[51] W. Deal, Y. Qian, T. Itoh, and V. Radisc, "Planar integrated antenna technology," *Channels*, vol. 4, p. 5G, Jul. 1999.
[52] L. Shuai, J. Ming, and Q. Xiaolin, "Joint polarization-DOA estimation using circle array," in *Proc. IET Conf. Publications*, 2009, pp. 1–5.
[53] J. Li, "Direction and polarization estimation using arrays with small loops and short dipoles," *IEEE Trans. Antennas Propag.*, vol. 41, no. 3, pp. 379–387, Mar. 1993.
[54] I. M. Amine and B. Seddik, "2-D DOA estimation using MUSIC algorithm with uniform circular array," in *Proc. 4th IEEE Int. Colloq. Inf. Sci. Technol. (CiSt)*, Oct. 2016, pp. 850–853.
[55] P. Stoica, T. Söderström, and V. Šimonyt, "On estimating the noise power in array processing," *Signal Process.*, vol. 26, no. 2, pp. 205–220, Feb. 1992.
[56] J. Nikonowicz, A. Mahmood, E. Sisinni, and M. Gidlund, "Quantitative benchmarks and new directions for noise power estimation methods in ISM radio environment," 2017, *arXiv:1711.05642*.
[57] Y. Dodge, *The Concise Encyclopedia of Statistics*. Cham, Switzerland: Springer, 2008.
[58] C. G. Ding, "Algorithm as 275: Computing the non-central χ^2 distribution function," *J. Roy. Stat. Soc., Ser. C, Appl. Statist.*, vol. 41, no. 2, pp. 478–482, 1992.
[59] N. L. Johnson, S. Kotz, and N. Balakrishnan, *Continuous Univariate Distributions*, vol. 2. Hoboken, NJ, USA: Wiley, 1995.
[60] J. M. Borwein and P. B. Borwein, "Pi and the AGM: A study in analytic number theory and computational complexity," *Bull. Amer. Math. Soc.*, vol. 22, pp. 198–201, Jan. 1990.
[61] R. P. Brent and P. Zimmermann, *Modern Computer Arithmetic*, vol. 18. Cambridge, U.K.: Cambridge Univ. Press, 2010.
[62] E. A. Santiago and M. Saquib, "Noise subspace-based iterative technique for direction finding," *IEEE Trans. Aerosp. Electron. Syst.*, vol. 49, no. 4, pp. 2281–2295, Oct. 2014.

MD IMRUL HASAN (Student Member, IEEE) received the B.Sc. degree from the Bangladesh University of Engineering and Technology (BUET), in 2016, and the master's degree in electrical engineering from The University of Texas at Dallas (UT Dallas), in 2022, where he is currently pursuing the Ph.D. degree. His research interests include signal processing for next-generation radar and wireless communication systems.

MOHAMMAD SAQUIB (Senior Member, IEEE) received the B.Sc. degree from the Bangladesh University of Engineering and Technology, Bangladesh, in 1991, and the M.S. and Ph.D. degrees from Rutgers University, New Brunswick, NJ, USA, in 1995 and 1998, respectively, all in electrical engineering. He worked as a member of the Technical Staff with the Massachusetts Institute of Technology Lincoln Laboratory, and an Assistant Professor with Louisiana State University, Baton Rouge, LA, USA. He is currently a Professor with the Electrical Engineering Department, The University of Texas at Dallas, Richardson, TX, USA. His current research interests include the various aspects of wireless data transmission, radio resource management, and signal processing techniques for low-cost radar applications.